united nations
educational, scientific
and cultural
organization

international atomic
energy agency

the
abdus salam
international centre for theoretical physics

SMR 1216 - 10

Joint INFM - the Abdus Salam ICTP School on
"Magnetic Properties of Condensed Matter Investigated by Neutron Scattering and Synchrotron Radiation Techniques"

1 - 11 February 2000

Background Material

"ULTRAFAST MAGNETIC DYNAMICS"

H.C. SIEGMANN
ETH - Zürich
Laboratorium für Festkörperphysik
CH-8093 Zürich, Switzerland

195

Reprinted from

journal of magnetism and magnetic materials

Journal of Magnetism and Magnetic Materials 200 (1999) 774–785

Ultrashort magnetic field pulses and the elementary process of magnetization reversal

C.H. Back, H.C. Siegmann*

Laboratorium für Festkörperphysik, ETH-Hongr, HPF D9, CH-8093 Zürich, Switzerland

Received 19 January 1999

ELSEVIER

JOURNAL OF MAGNETISM AND MAGNETIC MATERIALS

Aims and Scope
The *Journal of Magnetism and Magnetic Materials* provides an important forum for the disclosure and discussion of original contributions covering the whole spectrum of topics, from basic magnetism to the technology and applications of magnetic materials and magnetic recording. The journal encourages greater interaction between the basic and applied subdisciplines of magnetism, with short but comprehensive review articles, a rapid publication channel with *Letters to the Editors*, and a section *Information Storage: Basic and Applied* on all topics in magnetic and magneto-optic recording media and processes – in addition to full-length contributions.

Abstracted/indexed in:
Current Contents: Physical, Chemical and Earth Sciences; EI Compendex Plus; Engineering Index; INSPEC; Metals Abstracts

Subscription Information 1999
Volumes 191–205 of the *Journal of Magnetism and Magnetic Materials* (ISSN 0304-8853) are scheduled for publication. (Frequency: semimonthly; total 24 issues.)
Prices are available from the publishers upon request. Subscriptions are accepted on a prepaid basis only. Issues are sent by SAL (Surface Air Lifted) mail wherever this service is available. Airmail rates are available upon request. Please address all enquiries regarding orders and subscriptions to the Customer Support Department at the Regional Sales Office nearest to you (see journal front pages). Claims for issues not received should be made within six months of our publications (mailing) date.

US Mailing notice – The *Journal of Magnetism and Magnetic Materials* (ISSN 0304-8853) is published semimonthly (total 24 issues) by Elsevier Science B.V., Molenwerf 1, P.O. Box 211, 1000 AE Amsterdam, The Netherlands. Annual subscription price in the USA is US$ 5326 (valid in North, Central and South America only), including air speed delivery. Second class postage paid at Jamaica, NY 11431.
USA Postmasters: Send changes to Journal of Magnetism and Magnetic Materials, Publications Expediting, Inc., 200 Meacham Avenue, Elmont, NY 11003. Airfreight and mailing in the USA by Publications Expediting.

♾ The paper used in this publication meets the requirements of ANSI/NISO Z39.48-1992 (Permanence of Paper).

Printed in The Netherlands

North-Holland, an imprint of Elsevier Science

ELSEVIER

Journal of Magnetism and Magnetic Materials 200 (1999) 774–785

Journal of magnetism and magnetic materials

www.elsevier.com/locate/jmmm

Ultrashort magnetic field pulses and the elementary process of magnetization reversal

C.H. Back, H.C. Siegmann*

Laboratorium für Festkörperphysik, ETH-Hongr, HPF D9, CH-8093 Zürich, Switzerland

Received 19 January 1999

Abstract

Ultrashort magnetic field pulses can be generated in the final focus test beam facility at the Stanford Linear Accelerator. The 50 GeV electron bunches carrying currents up to 1000 A are squeezed through a focus smaller than 1 μm^2. The resulting magnetic field lines are equivalent to those of a straight current carrying wire with amplitudes up to 20 T and duration of 2–5 ps. These unique magnetic field pulses have been used to study magnetization reversal in thin films with in-plane and perpendicular easy magnetization directions. For perpendicular magnetized samples we observe ring domains with Kerr microscopy, which are reminiscent of the field contour during exposure. Their radii represent switching fields in quantitative agreement with the coherent rotation model. The broadening of the transition between oppositely magnetized domains can be attributed to the existence of static and dynamic fluctuations of the magnetic anisotropy. For films with an uniaxial anisotropy in the plane of the film we observe that smaller fields are sufficient to reverse the magnetization, provided the field is orthogonal to the magnetization. We show that it is the demagnetizing field that completes the reversal after the external field ceases to exist.

Keywords: Magnetization dynamics; Reversal processes; Magnetic anisotropy; Ultrashort magnetic field pulses

1. Introduction

The magnetization reversal process is essential to key technologies such as electric transformation or magnetic recording. The advancement in these fields motivates research in magnetization reversal at very short timescales below the nanosecond level. In high data rate magnetic recording, for instance, the data rate approaches 60 MB/s and thus magnetization reversal must take place in times approaching 1 ns. In the case of conventional magnetization reversal as practiced today the reversing field is applied antiparallel to the direction of the average magnetization $\boldsymbol{M}$. This means that the torque between the magnetization and the reversing field is minimal and temperature fluctuations or local deviations from the average magnetization direction initiate magnetization reversal. In general, magnetization reversal is governed by the sum of internal and external field contributions and thermal fluctuations (which can be viewed as a random field acting on the spins) [1,2]. A stable state is characterized by a minimum of the free energy. Magnetization reversal requires overcoming a barrier ΔE between adjacent minima.

*Corresponding author. Tel.: +411-633-2260/65; fax: +411-633-1080.

E-mail address: hcsieg@emlab.ethz.ch (H.C. Siegmann)

0304-8853/99/$ - see front matter
PII: S0304-8853(99)00313-3

At $T = 0$ the energy needed has to be supplied by an external magnetic field. At finite temperature T, thermal fluctuations help to overcome ΔE and thus magnetization reversal becomes temperature assisted [1,2]. The process is now of statistical nature if the external field is smaller than the maximum field at $T = 0$. To account for the statistical process Street and Wooley [3] have postulated a characteristic 'wait time' τ according to $1/\tau = f_0 \exp(-\Delta E/kT)$. Here $f_0 = 1/\tau_0$ is an attempt frequency which is of the order of 10^9–10^{12} 1/s [1,4,5] and depends in a non-trivial fashion on variables like anisotropy constant, magnetization, and damping [2–4]. In a simple approach it may be viewed as being connected to the characteristic time needed for energy exchange between lattice and spin, i.e. the spin lattice relaxation time τ_{sl} [6,7].[1] Recent experiments indicate values of $\tau_0 \cong 4 \times 10^{-9}$ s for small ferromagnetic particles [8,9] and $\tau_0 \cong 1 \times 10^{-9}$ s for particulate magnetic recording media [10]. Koch and co-workers [11] recently reported of switching in soft magnetic material indicating τ_0 somewhat below 1 ns. To eliminate temperature effects one considers experiments on time scales much shorter than τ_{sl}. In this case lattice and spins are decoupled and thermal activation ceases to exist. Thus the motion of the magnetization vector should simply follow the Landau–Lifshitz (LL) equation at $T = 0$. In this case reversal is governed solely by the field contributions. Successful reversal now depends on the length, strength and the direction of the applied magnetic field pulse. It was shown recently that magnetization reversal below the spin lattice relaxation time τ_{sl} is feasible if the external magnetic field $\boldsymbol{H}_{ex}$ inducing the reversal is applied perpendicular to $\boldsymbol{M}$ [12–14]. In that case, the torque $\boldsymbol{T} = \boldsymbol{H}_{ex} \times \boldsymbol{M}$ is maximum and angular momentum is directly transferred from the magnetic sample to the source of the magnetic field, such as the magnetic recording head. No fundamental limit seems to exist for the time of reversal. These non-stationary experiments are equivalent to experiments at $T = 0$ as energy transfer between the spin system and the phonon lattice is zero. These novel magnetic switching experiment also differ from FMR measurements where a small (as compared to the intrinsic fields) RF excitation causes coherent precession of the magnetic moments around a constant effective field composed of internal and external field contributions [15]. Because FMR is a stationary process it does not yield any information about the contribution of thermal activation and its variable impact on the magnetic reversal process for different excitation times.

In this paper we summarize magnetic switching experiments performed at times below τ_{sl}. We report of experiments with both, perpendicular and in-plane magnetized magnetic films and thus gain insight on the influence of the angle between the magnetization $\boldsymbol{M}$ and the applied field pulse $\boldsymbol{H}$. We show that the simple model of coherent rotation is sufficient to describe the basics of the switching dynamics. However, deviations from the simple model and their implications for magnetic recording are discussed. We believe that the experiments described here may lead to new insights in micromagnetic theory and eventually will aid ultrafast magnetic recording at time scales far below 1 ns. The paper is organized as follows. In Section 2 we describe the sample properties. In Section 3 we comment on the production of the strong magnetic fields on picosecond time scales using the Final Focus Test Beam facility at the Stanford Linear Accelerator. We shortly introduce the Landau–Lifshitz equation in Section 4. Section 5 summarizes experiments performed with perpendicularly magnetized samples, while Section 6 descirbes the work with films magnetized in the plane of the film. In Section 7 we summarize our results and comment on the implications for magnetic recording.

2. Sample properties

The experiment requires rather thin ferromagnetic films as the skin depth for the penetration of $\boldsymbol{H}_{ex}$ into a metal is ≈ 300 nm for a rise time of 1 ps. The thicknesses of the samples fulfill this requirement as they range between 20 and 24 nm. For the experiments using perpendiculary magnetized samples we use both, Co/Pt multilayers and Co/Pt

[1] Values for τ_{sl} are found to lie in the 100 ps range.

alloy samples. The polycrystalline thin film samples are e-beam evaporated $10 \times$ [Co x nm/Pt 1.2 nm] multilayers ($x = 0.44, 0.47, 0.69, 0.89$ and 0.92 nm) grown at $\cong 200°C$ onto (1 1 1) textured, 20 nm thick Pt buffer layers deposited at 400°C onto SiN_x coated Si(1 0 0) substrates. Furthermore, we include a $Co_{28}Pt_{72}$ alloy sample with thickness of 12.5 nm, grown at 220°C by co-evaporation onto a 20 nm thick Pt seed layer on a fused silica substrate. All samples were capped with 2 nm of Pt at ambient temperature for corrosion protection. Besides in situ controlling thicknesses and compositions during growth using quartz microbalance monitors the samples were characterized with Rutherford back scattering spectrometry and X-ray diffraction (XRD). XRD reveals strong (1 1 1) texturing. Clear multilayer satellites are visible for the multilayer samples. XRD rocking curves of Pt and zero order Co–Pt peaks indicate narrow crystallite dispersion angles of $8 \pm 1°$. The average (Θ–2Θ XRD) grain size is 15 nm. Magnetic properties were established prior to the experiments by using vibrating sample and torque magnetometry as well as magneto-optic Kerr effect. Most relevant in conjunction with the present discussion is the effective magnetic anisotropy field $H_{Aeff} = H_A - M_s/\mu_0$ which may be viewed as the field needed to saturate the sample in the hard plane. H_{Aeff} was determined within $\pm$ 10% accuracy and increases with decreasing Co layer thickness. H_{Aeff} ranges from 1280 to 2560 kA/m. The alloy sample has an anisotropy of $H_{Aeff} = 1760$ kA/m. Coercive fields range between 100 and 280 kA/m, ensuring that a written domain pattern is stable enough to be read weeks after field exposure. The film for the experiment with in-plane magnetized material consists of Co. It is single crystalline and magnetically uniaxial with the easy direction of $\boldsymbol{M}$ in-plane. It was DC-magnetron sputtered at $\cong 40°C$ with a thickness of 20 nm onto a 10 nm Pt-buffer. The buffer layer was deposited onto a series of [Fe 0.5 nm/Pt 5 nm] layers deposited in turn onto a MgO(1 1 0) substrate at $\cong 500°C$ to ensure pure (1 1 0) growth [16]. The film was capped with 2 nm Pt for corrosion protection. The saturation magnetization at room temperature is $M_s = 1.7$ T. The uniaxial anisotropy field lying in the plane of the film is $H_A =$ 168 kA/m.

3. The magnetic field source

The realization of extremely short magnetic field pulses far below 1 ns, sufficiently strong to switch the magnetization of materials with large anisotropies, does not seem feasible at first glance. Earlier attempts to produce such fields have resulted in pulses of 50 ps duration, but with small peak amplitudes of about 0.8 kA/m [17]. Pioneering research on hard magnetic material and particulate media in the group of Doyle [18] showed reversal characteristics with field pulses of 160 kA/m strength, but at a duration of about 640 ps. Strong magnetic fields may be produced with dense electron pulses accelerated to high energies. The relativistic length contraction leads to short pulses in the laboratory frame. Extremely high electron densities are achieved with fully relativistic electrons. At low energies, such electron clouds would explode due to electrostatic repulsion. The experiments were performed at the focal point of the final focus test beam (FFTB) facility at the Stanford Linear Accelerator Center (SLAC). The final focus test beam is an external electron beam line from the SLAC linac [19]. It is designed to make use of the low emittance delivered by the damping rings. The linac beam, at 46.6 GeV, is directed at near-zero degrees into a five-stage beam line where a demagnification of more than 300 leads to spot sizes as small as 40 nm in the vertical plane. The beam line and its systems are designed to test the techniques needed to deliver beams to the interaction point of future linear colliders while maintaining the specifications for high luminosity. For our experiments we use slightly larger beams as described below. The pre-magnetized samples were mounted on a motorized x–y–z manipulator, which was stepped through the beam pipe synchronous to the 1 Hz repetition rate of the 46.6 GeV electron beam. Each sample was exposed several times at different locations allowing to investigate the influence of pulse length and number of repetitions on samples with identical anisotropy. Before each run the length of the beam pulse was selected and its x and y dimensions were determined at the sample location using the FFTB wire scanners [20]. The number of electrons per bunch was recorded on a shot to shot basis using two torroids in the beam line. The

Gaussian half-widths of the electron beam in the x and y directions were determined to be $\sigma_x = 3.8 \pm 0.4\,\mu m$ and $\sigma_y = 0.8 \pm 0.2\,\mu m$, respectively. The number of electrons per bunch was $(9.1 \pm 0.2) \times 10^9$. The temporal pulse lengths σ_t in the experiments were 2, 3 and 4.4 ps. They were calibrated with an error of about 15% by recording the synchrotron radiation in the north arc leading to the Stanford Large Detector [21]. The magnetic field $H_{ex}(x, y, t)$ produced by the electron beam moving essentially at the speed of light is computed from the current density $j(x, y, t) = n(x, y, t) \cdot e \cdot c$ by simply applying Ampere's law. Here $n(x, y, t)$ is the number of electrons at a given position and time, determined by the three-dimensional Gaussian beam. The electromagnetic fields in the wake of the electron pulse generate considerable destruction in the thin film samples. Both the permanent and transient damage manifest themselves in the evaporation of atoms and heating to temperatures above the Curie-point, but the damage is limited to distances of a few micron from the center of impact [12,13]. Every point in the x–y plane perpendicular to the electron beam receives a magnetic field pulse of the same duration determined by the choice of σ_t. The direction of the magnetic field $\boldsymbol{H}_{ex}$ is, in good approximation at $R \geqslant 10\,\mu m$, perpendicular to the radius vector $\boldsymbol{R}$ and its strength decreases with $1/R$. Large fields up to 20 T are reached close to the surface of the beam. Weeks after exposure the samples were retrieved from the FFTB for further investigation.

4. The Landau–Lifshitz equation

A simple micromagnetic model can be applied to understand the switching behavior. The model is based on the Landau–Lifshitz equation

$$\frac{d\boldsymbol{M}}{dt} = -|\gamma|(\boldsymbol{M} \times \boldsymbol{H}_{tot}) + \frac{\alpha}{M}\left(\boldsymbol{M} \times \frac{d\boldsymbol{M}}{dt}\right).$$

The first term describes the precession of the magnetization in the magnetic field, with γ being the gyromagnetic ratio ($\gamma = 0.2212 \times 10^6$ (m/As)). The second term describes the rotation of the magnetization into the direction of the field due to energy dissipation and is characterized by the damping constant α. The total magnetic field is the sum of the beam field, the demagnetizing field, and the anisotropy field, $\boldsymbol{H}_{tot} = \boldsymbol{H}_{ex} + \boldsymbol{H}_D + \boldsymbol{H}_A$. In the case of the perpendicularly magnetized samples, the anisotropy field and the demagnetizing field point into the same direction and are represented by an effective anisotropy field $\boldsymbol{H}_{Aeff}$.

For the calculation of images the sample is subdivided into a square mesh, each cell having the same magnetization before the Gaussian beam pulse generated by the electron beam is applied. Both exchange and dipolar interactions between the cells are neglected. It will be shown, that this simple model is sufficient to understand the basics of the switching process.

5. Perpendicularly magnetized samples

In this section we summarize experiments performed with samples that have an easy magnetization direction pointing out of the plane of the film [12,13]. We apply a short but strong magnetic field pulse $\boldsymbol{H}_{ex}$ (in fact the field pulse is shorter than the time scale given by the precessional frequency of the magnetic sample. $\boldsymbol{H}_{ex}$ lies in the plane of the film and is perpendicular to the initial magnetization direction. In this particular geometry reversal occurs by precession of the magnetization vector while $\boldsymbol{H}_{ex}$ acts. The magnetization precesses below the plane defined by the film and then, on a much longer time scale, precesses around $\boldsymbol{H}_{Aeff}$ into the opposite easy magnetization direction. For successful reversal the magnetization must precess by an angle $\Phi \geqslant \pi/2$. This immediately means that damping effects can be neglected [22]. In this experiment we provide a rigorous test of the Stoner Wohlfarth model at picosecond time scales by varying two crucial parameters: pulse duration and strength of the anisotropy field. A quantitative comparison of the observed domain patterns with a LL-based calculation shows that the coherent rotation model applies even for continuous highly exchange coupled ferromagnetic films. Of particular interest is the sharpness of the transition region between up and down magnetized domains: its width cannot be explained in this model, and we postulate that the

observed broadening may be related to anisotropy fluctuations. This intrinsic broadening effect poses a fundamental limitation to high data rate magnetic recording.

After exposure the samples were retrieved from the FFTB and the magnetic domain patterns were examined in a Kerr microscope [23]. Fig. 1a shows a Kerr micrograph of a pattern written with a single 2 ps pulse into a Co/Pt multilayer sample with $H_{Aeff} = 2560$ kA/m, that had been pre-magnetized along the $-z$-axis. Fig. 1b shows a corresponding linescan along the y-direction at $x = 0$. Clearly five regions can be distinguished. Region I far away from the center is still magnetized along its original direction represented by a white contrast and the value $-M$ in the linescan. The dark ring of region II represents an area where the magnetization has switched at a corresponding maximum magnetic field at H_0 of 2090 kA/m and is now pointing along the $+z$ direction ($H(t) = H_0 e^{-t^2/2\sigma_t}$) (Fig. 2), In region III, even closer to the

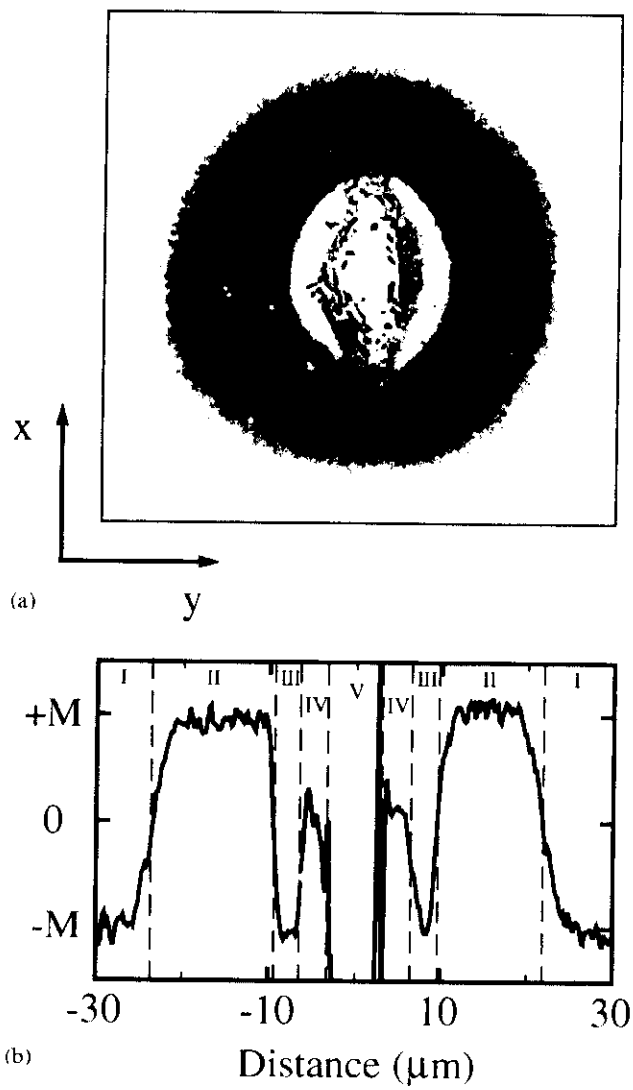

Fig. 1. (a) Domain pattern written into a Co/Pt multilayer with H_{Aeff} of 2560 kA/m and with $\sigma_t = 2$ ps. (b) Linescan along the y-direction through the center of the image.

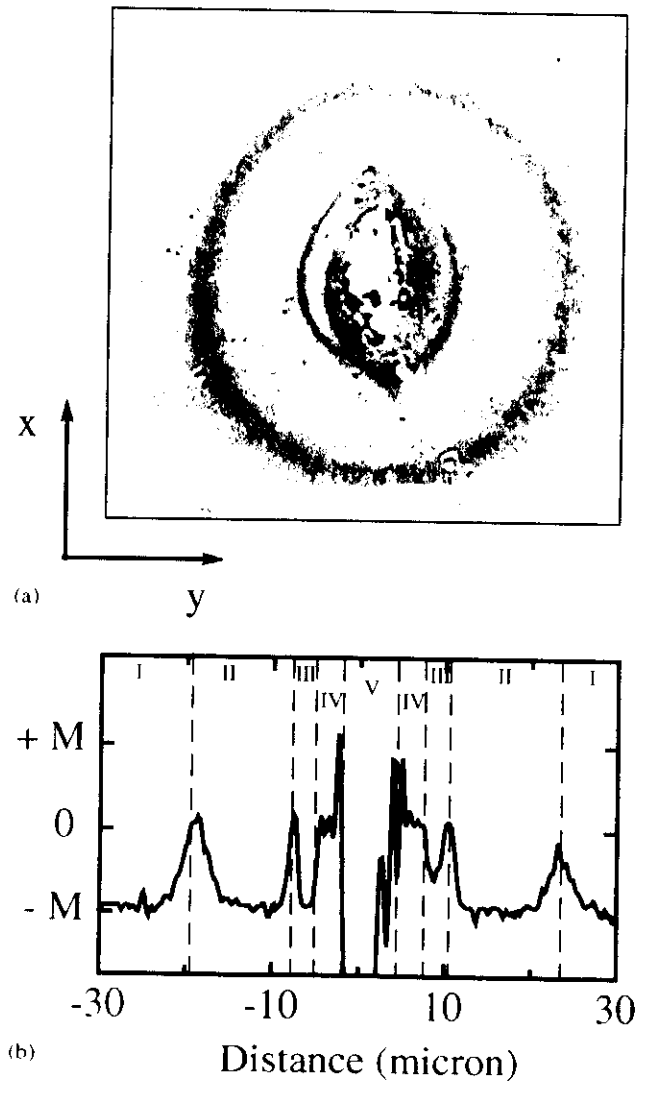

Fig. 2. (a) Domain pattern written into the same sample as in Fig. 1. The sample was exposed to two consecutive field pulses with $\sigma_t = 2$ ps. (b) Linescan along the y-direction through the center of the image.

core of the electron beam the magnetic field pulse was strong enough ($H_0 = 4970$ kA/m) to cause a second reversal of the magnetization direction which now points back into the $-z$-direction. This region is followed by an area with zero net magnetization – region IV – and correspondingly the contrast appears grey in the image. Region V represents the actual area of impact of the electron beam. The 46.6 GeV beam has evaporated the surface material and caused a crater of several micron depth. Region IV has been demagnetized. High-resolution Kerr microscopy in this region indicates the presence of magnetic domains with average size of 0.3–0.5 μm. The domains are not resolved in the shown Kerr micrograph and thus zero net magnetization is recorded. What is the cause of the domain formation? Heating the sample above its Curie temperature of about 500 K may cause demagnetization. Less than 1% of the beam energy is dumped into the material and a cylindrical heat wave is formed around the path of the electron beam. Based on a simple heat transport calculation we conclude that the Curie temperature cannot be reached at the border line of region IV. However, it is known that the electron beam can carry a halo of particles at very low particle density, below the detection limit of the gamma-ray detectors of the FFTB wire scanners, which can easily account for overheating. To investigate this problem we have – in a separate experiment – exposed a sample to a beam with the same number of electrons and the same pulse length, but with a different shape in the x–y plane. For this particular exposure we use $\sigma_x = 3.5 \pm 0.4$ μm and $\sigma_y = 0.2 \pm 0.2$ μm. The number of electrons per bunch was $(6 \pm 0.2) \times 10^9$. The Kerr micrograph (Fig. 3) shows a pattern written with a single 3 ps pulse into the $Co_{28}Pt_{72}$ alloy sample with $H_{Aeff} = 1760$ kA/m, that had also been pre-magnetized along the $-z$-axis. The beam in this experiment was known to have a larger background level of particles along the x-direction. In this test exposure the size of heated area near the center of impact increased along the x-direction to the extent that region II vanished completely along x. For this sample we also include a high-resolution Kerr micrograph that reveals the domain structure in the center and also

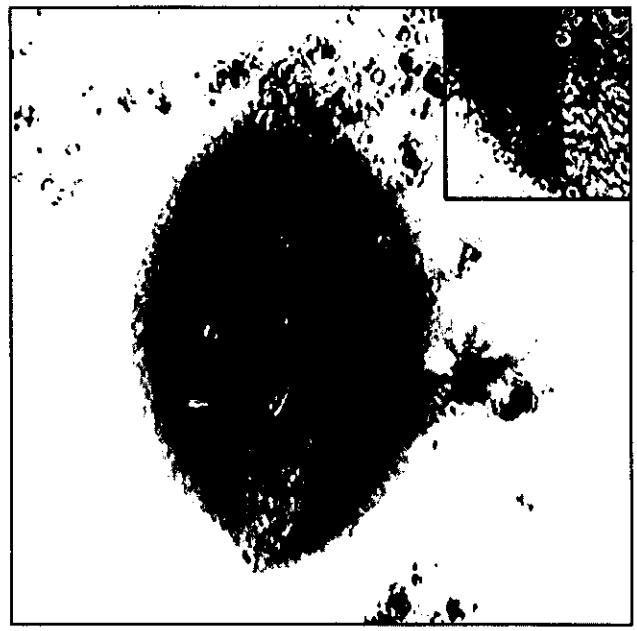

Fig. 3. Domain pattern written into a $Co_{28}Pt_{72}$ alloy sample with H_{Aeff} of 1760 kA/m. The field pulse lasted for 3 ps. The inset shows an enlarged area of the sample. Magnetic domains with an average size of 0.3–1.0 μm are clearly visible.

in the transition region between regions I and II, see inset.

A heat wave cannot be responsible for the multiple switching of regions II and III in Fig. 1a. To confirm this conclusion we have performed multiple shot experiments. One second elapsed between shots assuring a stable starting condition for the second shot. We show in Fig. 2a and the corresponding linescan in Fig. 2b, that the original magnetization state is reached as expected, except for the regions where domains have been formed after the first exposure.

Fig. 4 shows the calculated switching pattern for the film of Fig. 1a reproducing the observed gross features. We use $\sigma_t = 2$ ps, $\alpha = 0.1$, and $H_{Aeff} = 2560$ kA/m for the calculation. Fig. 5 summarizes calculated and measured switching radii for the set of multilayers at 2 ps pulse length. In Fig. 5a we plot switching radii versus the effective anisotropy. The experimental results agree well with the calculated values within the error bars which are mainly due to uncertainties in the pulse length. Fig. 5b displays the experimental and theoretical switching radii plotted versus pulse length at fixed

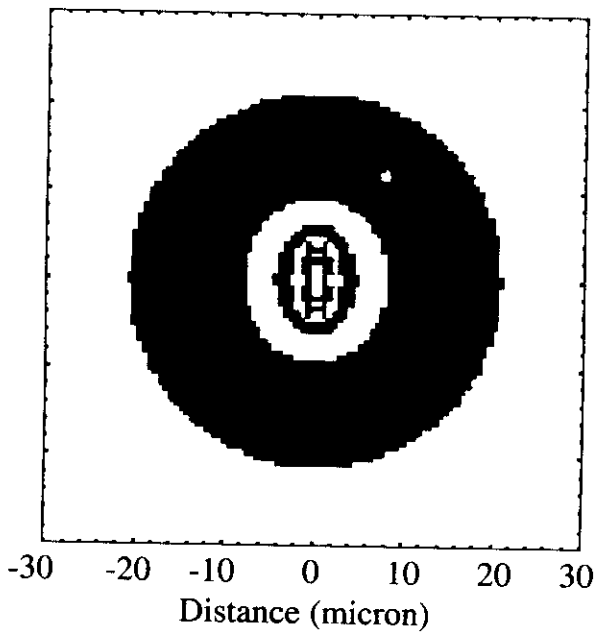

Fig. 4. Calculation of the domain pattern for the sample of 1(a) using the LL equation.

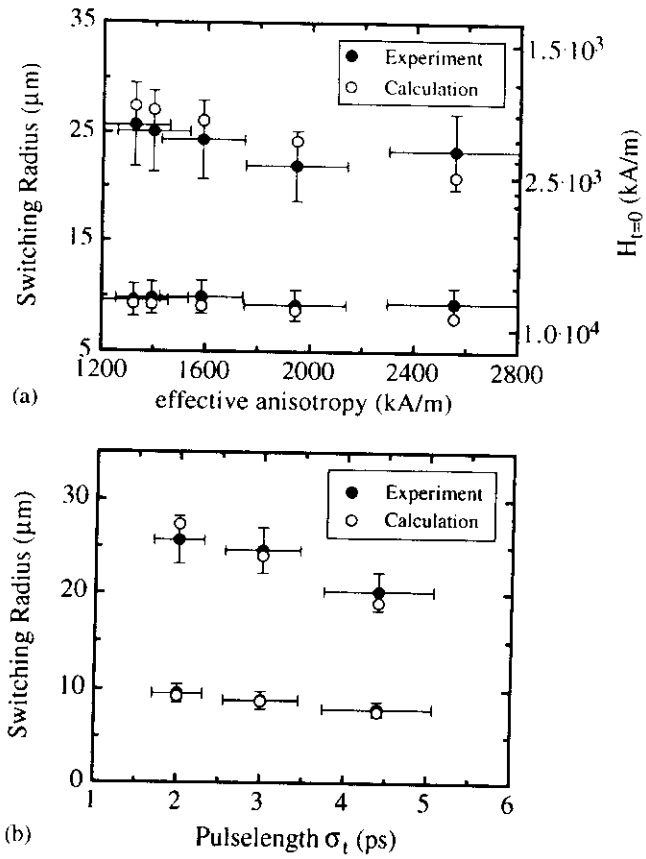

Fig. 5. (a) Measured (full circles) and calculated (open circles) switching radius in the y-direction and at $x = 0$ as a function of the strength of the anisotropy field for the Co/Pt multilayer samples. The lower points present data on the second switching closer to the region of impact. The axis to the right gives the corresponding magnetic field strength at $t = 0$. (b) Measured (full circles) and calculated (open circles) switching radius in the y-direction and at $x = 0$ as a function of the pulse duration for a sample with H_{Aeff} of 1320 kA/m.

$H_{Aeff} = 1320$ kA/m. Both, the first (between regions I and II) and second (between regions II and III) switch are included. Again good agreement is found. Fig. 6 summarizes measurements from different experiments using different pulse lengths, beam shapes and thin film samples, including alloys. The ratio of experimental and calculated switching radii is plotted. For all experiments the agreement is found to be better than 16% with the exception of the sample with the large anisotropy field of 2560 kA/m, where the discrepancy amounts to 40%. The agreement is in all cases within the experimental error. In the linescan in Fig. 1b one observes that the transition between the two states of magnetization is not sharp. One might think, that the spreading of the domains over 5 μm in the transition region between regions I and II can be explained by a non-uniform magnetization direction. If the magnetization direction in individual cells deviates statistically from the normal direction by a few degrees, the starting condition for spin rotation in each cell differs and a spread over a broad transition region can be expected. An average magnetization tilt angle away from the normal direction can be deduced from the measured ratio between remanent and saturation magnetization. The transition width can then be calculated, again using the LL equation. The results are shown in Fig. 7. The calculated transitions appear much narrower than the experimentally observed ones. To understand this we consider different effects of local lattice distortions. Deviations from the ideal lattice cause local changes of the electronic band structure, which via spin–orbit coupling modifies the magnetic anisotropy of a given material. For example strain of 1% in a Co single crystal may lead to changes in the magnetic anisotropy energy of up to 60%. Locally lattice strain can be caused

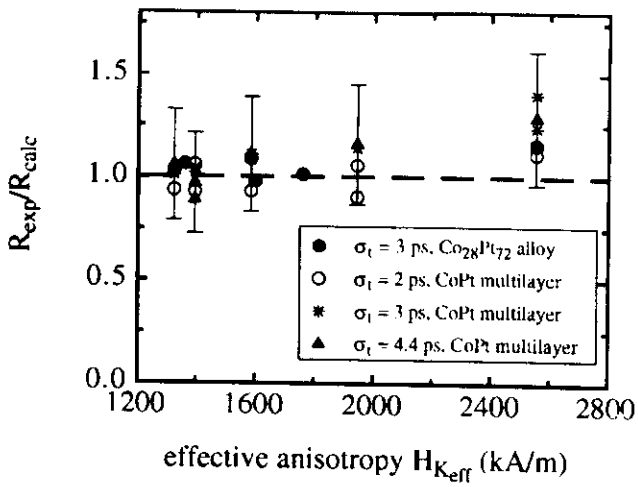

Fig. 6. Ratio of measured to calculated switching radius for all samples and all pulse durations. The broken line indicates the expectation based on the Stoner Wohlfarth model, which is 1.

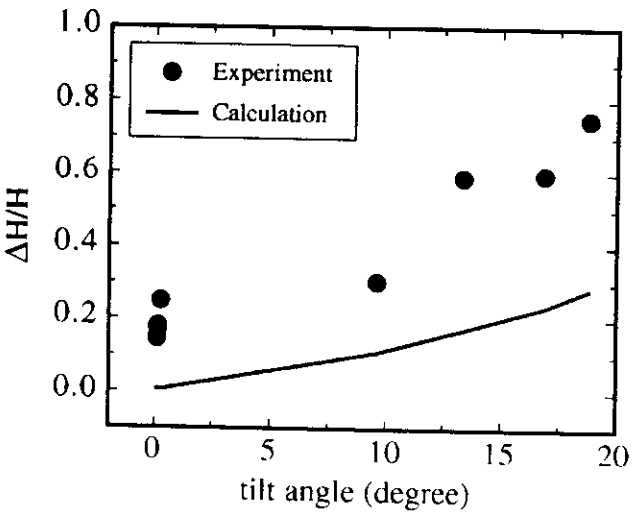

Fig. 7. Measured (full circles) and calculated (open circles) ratio of the width of the transition region to the transition radius versus the tilt angle of the magnetization direction away from the normal as deduced from the Kerr hysteresis loops.

by two mechanisms: (i) Local lattice imperfections caused by imperfect growth lead to a static variation of the value of the anisotropy field as a function of location. The strength of the anisotropy field may vary from cell to cell. A microscopic distribution of the strength of the anisotropy fields is not reflected in our macroscopic determination and may be responsible for the observed transition widths. (ii) At the time of the magnetic field excitation the lattice is frozen into a phonon distorted state. This leads to dynamic variations of the value of the anisotropy field as a function of location and time. Atomic distances vary locally causing variations of the anisotropy fields via spin–orbit coupling. The Debye–Waller yields an estimate of 5% for the lattice distortions caused by temperature. From our XRD measurements we conclude that the sum of static and dynamic distortions is of the order of 10–15%, thus static distortions are of the same magnitude or larger than dynamic distortions. Both effects lead to a distribution of initial anisotropies before the magnetic field pulse acts on the sample and this in turn results in a distribution of small up and down domains after the field pulse has passed. On a much longer time scale these domains then relax into domains of at least the size of the exchange length. This relaxation process does not affect the written domain pattern, but only the size of the domains in the transition region.

6. In-plane magnetized samples

In the preceeding section we have shown that ultrafast magnetization reversal utilizing the strong magnetic field pulses of the FFTB is feasible. However, the required magnetic field strength exceeds 2000 kA/m. In this section we demonstrate that considerably weaker field pulses are sufficient for reversing $\boldsymbol{M}$. This occurs in thin uniaxial films magnetized in the plane. We show that this is due to the demagnetizing field $\boldsymbol{H}_D$ brought about by the precession of $\boldsymbol{M}$ during the field pulse out of the plane of the film. When the external magnetic field pulse is terminated, $\boldsymbol{H}_D$ persists, and the precession of $\boldsymbol{M}$ around $\boldsymbol{H}_D$ completes the reversal. In this geometry, magnetization reversal is induced with magnetic field pulses of a few picoseconds' duration, but with small field amplitudes of $\cong 350$ kA/m. These field amplitudes are well within reach of conventional thin-film recording heads [24]. In contrast to conventional reversal and to the experiments described above with perpendicular films, the damping coefficient α describing the relaxation of $\boldsymbol{M}$ into the direction of the magnetic field is now the material parameter of crucial

importance. The full relaxation process has to be taken into account for the reversal process. As this takes much longer time compared to the case of perpendicularly magnetized samples, damping now starts to play a role. In fact the relaxation process now reaches timescales comparable to the spin–lattice relaxation time [6,7].

Again every point in the x–y plane perpendicular to the electron beam receives a magnetic field pulse of the same duration determined by the choice of σ_t. In this experiment, however, we utilize in-plane magnetized uniaxial films. Prior to exposure, the magnetization $\boldsymbol{M}$ of the films is set parallel to the x-direction. Hence the direction of the magnetic field $H_{ex}(x, y)$ encloses all angles $-\pi \leqslant \vartheta \leqslant +\pi$ with $\boldsymbol{M}$.

After exposure the samples are removed from the beam line. Magnetic information is again obtained in a Kerr microscope. Fig. 8a shows the magnetic pattern generated in the Co film by a single field pulse of $\sigma_t = 2$ ps duration. The initial magnetization direction points along $-x$ (white). Black contrast represents areas that have switched the magnetization direction from $-\boldsymbol{M}$ to $+\boldsymbol{M}$. The location of impact is at the center of the image, which we also define as the center of the coordinate system. The induced magnetization pattern is symmetric on changing the sign of x, but asymmetric on changing the sign of y.

We first concentrate on the line $y = 0$. On this line, $\boldsymbol{H}_{ex} \perp \boldsymbol{M}$ and the initial torque $\boldsymbol{T} = \boldsymbol{H}_{ex} \times \boldsymbol{M}$ is maximum. The first reversal is $x = 130$ μm from the center, corresponding to a magnetic field of $H_0 = 356$ kA/m. Towards $x = 0$, i.e. towards larger field values, multiple reversals occur at $x = 113.3$ μm ($H_0 = 409$ kA/m), $x = 97.5$ μm ($H_0 = 475$ kA/m), and $x = 73.9$ μm ($H_0 = 627$ kA/m). On the line with zero average torque $x = 0$ no reversal is observed outside the area of beam damage. This shows the fundamental difference between conventional magnetization reversal with $\boldsymbol{H}_{ex}$ antiparallel to $\boldsymbol{M}$ and UF reversal. In the case of UF reversal, the initial torque $\boldsymbol{T} = \boldsymbol{H}_{ex} \times \boldsymbol{M}$ is not equal to zero and is transferred directly from the magnetic sample to the source of the magnetic field, such as the magnetic recording head. No fundamental limit seems to exist for the time of reversal. On the other hand, in conventional magnetization reversal the average torque is equal to zero. In this case, the angular momentum induced by the reversal process must be absorbed by the phonon lattice, a process that is governed by the rate of energy exchange between the lattice and the magnetic system. Thus, the spin–lattice relaxation time is the relevant time scale for reversal [6,7]. The multiple reversals along $y = 0$ at larger field values hint at a second requirement for UF reversal: at a given pulse length the magnetic field strength must assume a value in a rather narrow interval, and the product $\sigma_t H_0$ becomes important. At this point we also stress the size of the magnetization pattern. Its diameter amounts to 230 μm, about a factor of 5 larger than

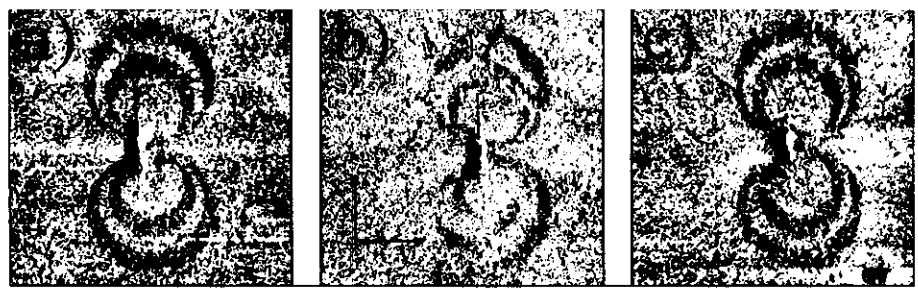

Fig. 8. (a) Magnetization pattern written into the uniaxial Co film with a single electron pulse with $\sigma_t = 2$ ps. The image was measured with a Kerr microscope, image size 290 μm × 290 μm. The sample was premagnetized along the $-x$ direction. In the light areas the magnetization points along the $-x$ direction, in the dark areas it has been reversed to the $+x$ direction. (b) Magnetization pattern written into the uniaxial Co film with two consecutive electron pulses each with $\sigma_t = 2$ ps. Some residual reversed magnetization is visible (dark areas). (c) Magnetization pattern written into the uniaxial Co film with three consecutive electron pulses each with $\sigma_t = 2$ ps. The pattern reverts back to that of Fig. 8a.

that observed for the perpendicularly magnetized samples in Ref. [13]. This indicates that the field strength which is required to reverse the magnetization with the same pulse length $\sigma_t = 2$ ps is considerably smaller for in-plane magnetized films, namely only 356 kA/m.

Fig. 8b shows the same Co film after exposure to two consecutive pulses separated by 1 s. The asymetry of the pattern after the first pulse now becomes more obvious. The second pulse cannot reverse the whole pattern as in the case of the perpendicularly magnetized samples. The third pulse shown in Fig. 8c reverts the pattern to that of a single pulse.

In order to understand the decrease of the applied magnetic field $\boldsymbol{H}_{ex}$ capable of reversing $\boldsymbol{M}$ for in-plane magnetized films consider a simple model. Let us consider a small, single particle that is symmetric in the xy-plane with a uniaxial anisotropy $\boldsymbol{H}_A$ along the x-direction. This particle may have any shape between a sphere and a thin disk. The corresponding demagnetizing field $\boldsymbol{H}_D$ results from the difference in the demagnetization factor $D_\parallel$ for $\boldsymbol{M}$ in the xy-plane and $D_\perp$ for $\boldsymbol{M}$ along the z-direction, $\boldsymbol{H}_D = (D_\perp - D_\parallel)M_s/\mu_0$. Let us assume coherent rotation of $\boldsymbol{M}$ in an external field pulse of Gaussian shape applied along the y-direction with an amplitude H_0 and duration σ_t. If the particle is a sphere, $D_\perp - D_\parallel = 0$ and hence $H_D = 0$. This means that for $H_0 \gg H_A$, precession of $\boldsymbol{M}$ around $\boldsymbol{H}_0$ takes place. For successful reversal the precession angle Φ must exceed $\pi/2$, with Φ given by the Larmor frequency. This limits the radius for successful reversal to $R_0 = 32$ μm. If we now fill the plane with decoupled spheres we obtain a figure-eight-shaped magnetization pattern according to $R = R_0 \sin(\vartheta)$, where ϑ is the angle between $\boldsymbol{M}$ and $\boldsymbol{H}$. We can now increase $D_\perp - D_\parallel$ from 0 to 1, the value for a film. The calculation for the magnetization reversal is now performed again using the Landau–Lifshitz (LL) equation for each individual particle. We use α as the only parameter to fit the size of the pattern of Fig. 8a and find $\alpha = 0.037$. Fig. 9 shows the results for the Co film along $y = 0$. It is seen that with increasing demagnetization factor and hence increasing $H_D = M_s/\mu_0$, the size of the pattern grows rapidly. Thus the demagnetizing field plays a crucial role in the reversal process.

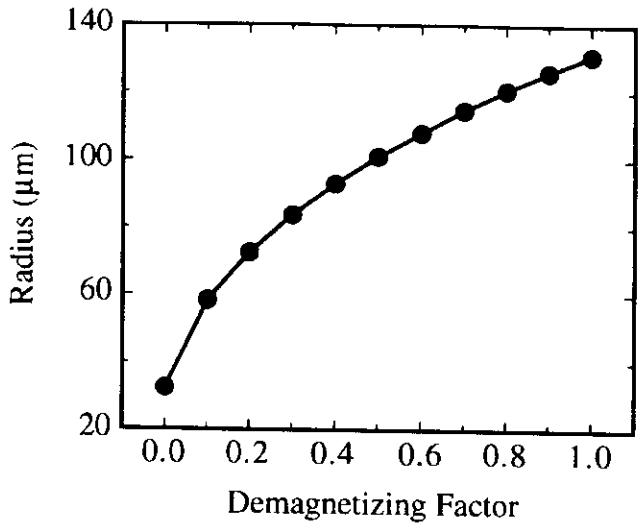

Fig. 9. Calculated distance of the first reversal along $y = 0$ versus the difference $D_\perp - D_\parallel$ of the demagnetization factors for $\boldsymbol{M}$ perpendicular and parallel to the plane of the film; $\alpha = 0.037$, $\sigma_t = 2$ ps.

This leads to the following three-step model for ultrafast reversal. (1) During the field pulse, $\boldsymbol{M}$ precesses around $\boldsymbol{H}_{ex}$ out of the plane of the film. As $\boldsymbol{M}$ leaves the plane of the film the effective demagnetizing field decreases with the angle Θ between $\boldsymbol{M}$ and the surface normal: $H_D = (M_s/\mu_0)\cos\Theta$. (2) When $\boldsymbol{H}_{ex}$ ceases to exist, $\boldsymbol{M}$ continues to precess, but now around $\boldsymbol{H}_D + \boldsymbol{H}_A$. The maximum angle Θ assumed by $\boldsymbol{M}$ decides whether the magnetization reverses and whether even multiple reversals can occur. (3) Eventually $\boldsymbol{M}$ relaxes into one of the two easy magnetization directions. This final step can be very slow.

The magnetization patterns thus obtained with the LL equation for the Co film is shown in Fig. 10b. We see that the size and the overall outer shape of the pattern is well reproduced by the calculation. The asymmetry of the pattern when y is inverted is caused by the direction of the premagnetization. A further test for the correct choice of α is the comparison of the experimental location of the first reversal with the calculated one when the duration of the field pulse is varied. The results are shown in Fig. 11, and good agreement is found for the parameter determined to match the size of the pattern.

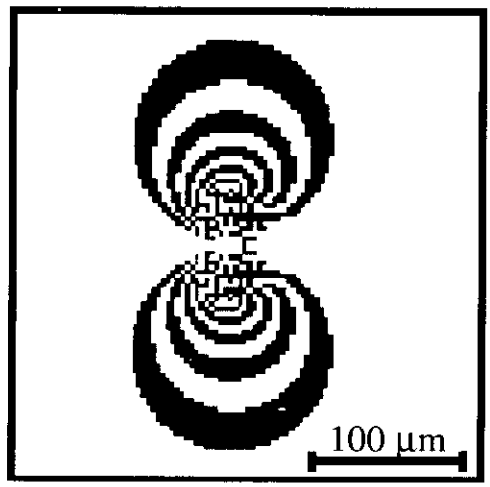

Fig. 10. Magnetization pattern calculated using the Landau–Lifshitz equation with $M_s = 1.7$ T, $H_A = 168$ kA/m, $\sigma_t = 2$ ps, and $\alpha = 0.037$.

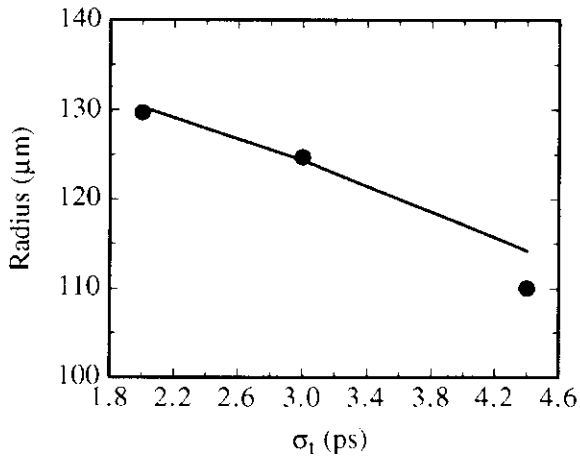

Fig. 11. Measured (full circles) and calculated values of the position of the first reversal along $y = 0$ versus the length of the magnetic field pulse σ_t. For the calculations we assume $M_s = 1.7$ T and $D_\perp - D_\parallel = 1$. We use $H_A = 168$ kA/m and $\alpha = 0.037$.

We note that the radii of the experimentally observed inner rings are not exactly reproduced by the calculations. For example the second reversal back to the original direction occurs at smaller field values than expected. The details of the inner structure of the pattern cannot be calculated with the simple LL approach unless one assumes that some of the material properties vary with time. Supposing that intrinsic properties such as M_s and H_A are constant, one is forced to assume that α is time-dependent. Two different mechanisms might lead to a time-dependent effective damping constant α_{eff}. The first one is the excitation of magnons. Field pulses are built with frequencies close to the frequency band of magnons, hence magnon excitation might be enhanced. This can lead to an increase in energy dissipation and thus to an increase in α_{eff}. The other mechanism is electron–electron scattering [25]. If $\boldsymbol{M}$ precesses at a different rate in each location, this scattering will be very strong, again leading to a larger effective damping constant.

7. Conclusions

Based on experimental advances, magnetization reversal has seen considerable development in recent years. For instance, it is now possible to observe the direction of the magnetization in nanosized single-domain particles [8,9,26]. In such experiments, static magnetic fields are applied for times typically of the order of 1 s. The probability of reversal of $\boldsymbol{M}$ is then determined as it depends on the angle at which the external magnetic field is applied to the particle. The reversal is difficult to understand in detail because $\boldsymbol{M}$ might assume complex curling and buckling modes depending on details of the surface and bulk anisotropy of the grain under investigation. Ultrafast reversal removes this problem as favorable curling and buckling modes need a comparatively long time to develop and may be neglected. Therefore, putting nanoparticles on a substrate and applying the ultrafast pulse is an interesting experiment that must still be done.

The present experiments would greatly gain in value by ultrafast observation of $\boldsymbol{M}$ as it precesses in the various steps of the reversal. Freeman and coworkers [17] have shown that this is indeed possible with the magneto-optic Kerr-effect using picosecond laser pulses. Another exciting prospect comes from the development of the Japan Linear Collider [27]. In this project, microstructured electron pulses will be developed delivering a train of

very strong magnetic field pulses with picosecond length, ideally suited for observing the dynamics of the reversal.

In conclusion, we have shown that magnetic switching in perpendicular and in-plane magnetized samples at ultra short times scales in the picosecond regime can be well understood within the simple LL-model. The width of the written transitions in perpendicularly magnetized films is not only determined by the quality of the magnetic material, but is ultimately determined by intrinsic physical properties such as phonons. The phonon-driven broadening of the transition region sets the ultimate limit for the transition density in ultrafast magnetic recording. We have also shown that it is possible to switch the magnetization of longitudinally magnetized magnetic films in much smaller magnetic fields. In this case the switching field is smallest when the field pulse is applied orthogonal to the initial magnetization direction of the sample and increases continuously as the angle between the applied field and the magnetization is reduced. In addition, we find that the magnitude of the switching field is strongly dependent on the damping parameter of the magnetic film [14].

These results have important implications for longitudinal magnetic recording and demonstrate the possibility of extremely high-data-rate recording if problems arising from transitions between regions of oppositely magnetized material can be overcome. This requires either a magnetic medium consisting of identical grains or single-domain particles.

Acknowledgements

We thank David W.G.S. Leith, director of research at SLAC and David L. Burke of the FFTB for supporting this project. We gratefully acknowledge the valuable input of a number of people at the FFTB and PEL, particularly C. Bula, G.J. Collet, C. Field, E.L. Garwin, F. King, and C.Y. Prescott. We also acknowledge the valuable input and discussions with a number of collaborators at IBM Almaden, IBM Zurich and the Swiss Federal Institute of Technology, namely R. Allenspach, D. Guarisco, J. Heidmann, D. Mauri, S.S.P. Parkin, W. Weber, and D. Weller. C.H.B. gratefully acknowledges the Swiss National Fund for financial support. This work was supported in part by the Department of Energy under contract DE-AC03-76SF00515.

References

[1] L. Néel, Ann. Geophys. 5 (1949) 99.
[2] W.F. Brown, Phys. Rev. 130 (1963) 1677.
[3] R. Street, J.C. Wooley, Proc. Phys. Soc. London, Sect. A 62 (1949) 562.
[4] P. Gaunt, J. Appl. Phys. 48 (1977) 3470.
[5] A. Lyberatos, R.W. Chantrell, J. Phys.: Condens. Matter 9 (1997) 2623.
[6] A. Vaterlaus et al., Phys. Rev. B 46 (1992) 5280.
[7] A. Scholl et al., Phys. Rev. Lett. 79 (1997) 5146, and references therein.
[8] W. Wernsdorfer et al., Phys. Rev. Lett. 78 (1997) 1791.
[9] M. Ledermann, S. Schultz, M. Ozaki, Phys. Rev. Lett. 73 (1994) 1986.
[10] L. He et al., J. Magn. Magn. Mater. 6 (1996) 155.
[11] R.H. Koch et al., Phys. Rev. Lett. 81 (1998) 4512.
[12] H.C. Siegmann et al., J. Magn. Magn. Mater. 151 (1995) L8.
[13] C.H. Back et al., Phys. Rev. Lett. 81 (1998) 3251.
[14] C.H. Back et al., in preparation.
[15] G.T. Rado, J. Appl. Phys. 32 (Suppl. 3) (1960) 129.
[16] D.J. Smith, A.R. Modak, T.A. Rabedeau, S.S.P. Parkin, Appl. Phys. Lett. 71 (1997) 1480.
[17] M. Freeman et al., IEEE Trans. Magn. 27 (1991) 4840.
[18] W.D. Doyle, L. He, P.J. Flanders, IEEE Trans. Magn. 29 (1993) 3634.
[19] Final Focus Test Beam Design Report, SLAC-376, March 1991, SLAC, Stanford.
[20] C. Field, Nucl. Instr. and Meth. A 360 (1995) 467.
[21] R. Holtzapple, FFTB log book, unpublished.
[22] L. He, W.D. Doyle, J. Appl. Phys. 79 (1996) 6489.
[23] W. Rave, R. Schaefer, A. Hubert, J. Magn. Magn. Mater. 65 (1987) 7.
[24] R. Wood, M. Williams, J. Hong, IEEE Trans. Magn. 26 (1990) 2954.
[25] D. Oberli et al., Phys. Rev. Lett. 81 (1998) 4228.
[26] S.Y. Chou, P.R. Krauss, L. Kong, J. Appl. Phys. 79 (1996) 6101.
[27] T. Nakanishi, Proceedings of LE '98, St. Petersburg, September 2–8, 1998.

JOURNAL OF MAGNETISM AND MAGNETIC MATERIALS

Instructions to Authors

Submission of papers

Manuscripts (one original + two copies), should be sent to one of the Editors (see addresses on inside front cover). Papers for the section *Information Storage: Basic and Applied* should be submitted to Prof. R.W. Chantrell. *Letters to the Editor* should be sent, preferably by fax, to one of the four editors, while the original with figures should be mailed to the Publisher (see address opposite), preferably with the source file included on disk. Letters may not exceed six pages when printed and will be given priority in both the refereeing and production processes. The faster production schedule may preclude sending proofs of letters to authors.

Original materials: Submission of a manuscript implies it is not being simultaneously considered for publication elsewhere and that the authors have obtained the necessary authority for publication.

Manuscript preparation

All manuscripts should be written in good English. The paper copies of the text should be prepared with double line spacing and wide margins, on numbered sheets. See notes opposite on the electronic version of manuscripts.

Structure: Please adhere to the following order of presentation: Article title, Author(s), Affiliation(s), Abstract, PACS codes and keywords, Main text, Acknowledgements, Appendices, References, Figure captions, Tables.

Corresponding author. The name, complete postal address, telephone and fax numbers and the e-mail address of the corresponding author should be given on the first page of the manuscript.

PACS codes/keywords. Please supply one or more relevant PACS-1995 classification codes and about 5 keywords of your own choice for indexing purposes.

References. References to other work should be consecutively numbered in the text using square brackets and listed by number in the Reference list. Please refer to recent issues for examples.

Illustrations

Illustrations should also be submitted in triplicate: one master set and two sets of copies. The *line drawings* in the master set should be original laser printer or plotter output or drawn in black india ink, with careful lettering, large enough (3–5 mm) to remain legible after reduction for printing. The *photographs* should be originals, with somewhat more contrast than is required in the printed version. They should be unmounted unless part of a composite figure. Any scale markers should be inserted on the photograph itself, not drawn below it.

Colour plates. Figures may be published in colour, if this is judged essential by the Editor. The Publisher and the author will each bear part of the extra costs involved. Further information is available from the Publisher.

After acceptance

Notification. You will be notified by the Editor of the journal of the acceptance of your article and invited to supply an electronic version of the accepted text, if this is not already available.

Copyright transfer. In the course of the production process you will be asked to transfer the copyright of the article to the Publisher. This transfer will ensure the widest possible dissemination of information.

Electronic manuscripts

The Publisher heartily welcomes the receipt of an electronic version of your accepted manuscript. If there is not already a copy of this (on diskette) with the Journal Editor at the time the manuscript is being refereed, you will be asked to send a file with the text of the accepted manuscript directly to the Publisher by e-mail or on diskette to the address given below. (When e-mailing a non-ASCII word-processor file, you should send it as an e-mail attachment). The name and version of the word-processing program and the type of operating system should always be indicated. Please note that no deviations from the version accepted by the Editor of the journal are permissible without the prior and explicit approval by the Editor. Such changes should be clearly indicated on an accompanying printout of the file.

Author benefits

No page charges. Publishing in the *Journal of Magnetism and Magnetic Materials* is free.

Free offprints. The corresponding author will receive 25 offprints free of charge. An offprint order form will be supplied by the Publisher for ordering any additional paid offprints.

Discount. Contributors to Elsevier Science journals are entitled to a 30% discount on all Elsevier Science books.

Further information (after acceptance)

Elsevier Science B.V.
Issue Management
Journal of Magnetism and Magnetic Materials
P.O. Box 2759, 1000 CT Amsterdam
The Netherlands
Fax: + 31 20 485 2319
e-mail: h.arends@elsevier.nl

North-Holland, an imprint of Elsevier Science

Total Scattering Cross Section and Spin Motion of Low Energy Electrons Passing through a Ferromagnet

D. Oberli, R. Burgermeister, S. Riesen, W. Weber, and H. C. Siegmann
Laboratorium für Festkörperphysik, ETH Zürich, CH-8093 Zürich, Switzerland
(Received 10 June 1998)

It is shown that the spin asymmetry of the elastic transmission of electrons through ferromagnetic films can approach unity. The polycrystalline Co films are a few nanometers thick and saturated with the magnetization $\vec{M}$ in the plane. The contribution of spin-productive scattering events is below 5%. If the electron spin at incidence is chosen to be perpendicular to $\vec{M}$, it rotates into the direction of $\vec{M}$ and also precesses around it. [S0031-9007(98)07521-8]

PACS numbers: 73.50.Yg, 79.20.Kz

The application of polarized electron beams to the study of magnetism took its beginning when the first spin-polarized electrons were obtained by photoemission from magnetic materials [1]. The most obvious way of looking at photoemission of electrons theoretically is to assume that the fast photoelectron does not interact appreciably with the other electrons in the metal so that the photoemission experiment often is thought of as measuring the energy spectrum of its own hole state left behind. This theory of renormalized one-electron states has been discussed in the present context by Anderson [2], Doniach [3], Gutzwiler [4], and many others [5]. However, it could never explain the fact that no negative spin polarization is detected in photoemission from states near the Fermi energy E_F in Co [6,7]. This and many other features observed in emission of low energy electrons from transition metals are now understood by considering the scattering of the excited electron on the partially filled d states of *all* of the atoms encountered in transport through the transition metal [8]. To study this important phenomenon more thoroughly, we have measured the total scattering cross section as a function of electron energy. In contrast to numerous earlier investigations [9], we have observed very large transmission asymmetries A of up to 80% with an electron beam passing through a thin ferromagnet depending on whether its spin is parallel or antiparallel to the magnetization $\vec{M}$. Furthermore, when the spin polarization vector $\vec{P}_0$ of the incident electron beam is chosen to be perpendicular to $\vec{M}$, then it rotates into the direction of $\vec{M}$ and simultaneously also precesses around $\vec{M}$. There is a complete analogy to the magneto-optic phenomena observed when a light beam passes through ferromagnetic material. But, even when measured on the length scale of the penetration depth, the magneto-"optic" effects observed with electron beams are at least 1 order of magnitude larger as compared to those observed with light beams. This arises because the electron beam couples directly to the magnetization, while the coupling of the light beam must be mediated by the spin-orbit interaction. The observations presented here have a number of immediate important implications. For instance, the scattering cross section governs the nonequilibrium magnetization dynamics which is presently at the forefront of fundamental research in magnetism [10–13]. Furthermore, experiments of the type described here might help to improve the performance of spin filters, spin transistors, and spin tunneling, and may also lead to magnetic imaging in transmission electron microscopy.

The experiment is sketched in the upper part of Fig. 1. We have prepared a spin-modulated electron beam with a GaAs-type photocathode. By switching from right- to left-circularly polarized light for excitation of the source, we can invert the vector $\vec{P}_0$ of the spin polarization. By applying a combination of electric and magnetic fields to

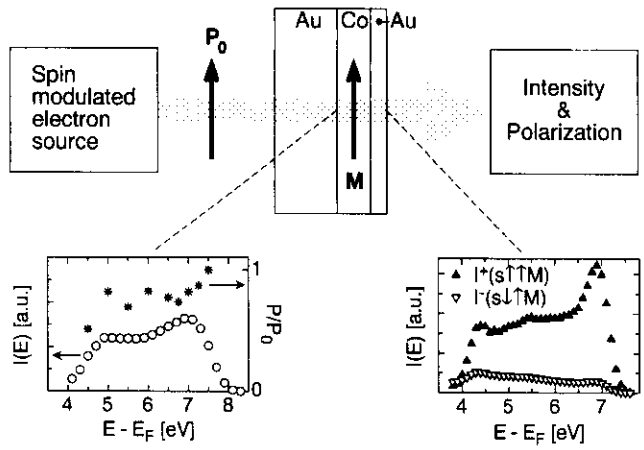

FIG. 1. The upper part shows the principle of the experiment consisting of a spin-modulated electron source of the GaAs type, a Au/Co/Au trilayer in which the ferromagnetic polycrystalline hcp Co film is magnetized remanently in the plane, and a detection system in which the intensity I and degree of spin polarization P perpendicular to the axis of the electron beam are measured for the electrons transmitted by the trilayer. The lower part shows on the left the energy distribution curve $I(E)$ and the degree of relative polarization P/P_0 after the electron beam has traversed the supporting Au layer alone. P_0 is the degree of spin polarization delivered by the source. In the lower part on the right, the intensity distribution curves $I^+(E)$ and $I^-(E)$ are shown for a Co film of 4 nm thickness and its 2 nm thick Au capping added. $I^+(E)$ is valid for spin parallel to the magnetization $\vec{M}$, and $I^-(E)$ for spin antiparallel to $\vec{M}$.

 0031-9007/98/81(19)/4228(4)$15.00

the electron beam, we can also rotate $\vec{P}_0$ into any desired direction in space. We can produce an unpolarized electron beam as well by applying linearly polarized light.

The spin-polarized electron beam impinges along the surface normal onto a trilayer consisting of a supporting Au film 20 nm thick, a ferromagnetic Co layer of varying thickness ranging from 1–6 nm, and a capping Au layer of 2 nm thickness to prevent corrosion. In this geometry spin-orbit coupling cannot produce any spin dependence of the transmission.

The trilayer is made in a separate chamber on a substrate consisting of a film of nitrocellulose supported by a Si wafer with a number of 0.5 mm wide apertures. The Au layer of 20 nm thickness is deposited on top of the nitrocellulose by evaporation of Au from a heated Mo crucible. On top of this layer, polycrystalline films of hcp Co are deposited by electron bombardment of a 99.998% pure Co rod. Their thickness (as measured by a calibrated quartz microbalance) ranges from 1–6 nm. The Co films are capped with a protecting Au layer of 2 nm thickness. The first set of hysteresis loops is measured right after deposition by *in situ* Kerr magnetometry. The in-plane hysteresis loops are square and exhibit full magnetic remanence. After the magnetic tests are completed, the whole sample is let to air. The nitrocellulose on the apertures is removed in a solution of pentyl acetate. The sample is then introduced through a load-lock system into the chamber with the GaAs electron source where the measurements are done. There, the sample is first exposed to mild sputtering designed to get rid of the contaminants acquired in the process of letting it to air and dissolving the nitrocellulose. Further sputtering through the apertures thins the supporting Au layer until electrons of a primary energy of ~6 eV above E_F are transmitted at an attenuation of 10^{-5}–10^{-6}. The final thickness of the supporting Au layer is estimated at ~18 nm. The Kerr hysteresis loops taken later show no difference to the loops obtained just after deposition of the samples.

In the actual measurements, the Co films are remanently magnetized in the plane by applying a positive or negative magnetic field pulse. The electrons emerging from the Au/Co/Au multilayer are energy analyzed by a retarding field, and subsequently accelerated to an energy of 100 keV to determine the components of the spin polarization vector perpendicular to the axis of the electron beam via Mott scattering.

In the lower part of Fig. 1 we show data observed with an incident electron beam of about 7 eV energy and $\vec{P}_0$ perpendicular to the electron beam. The inset on the left shows intensity and polarization as a function of energy without the Co film in order to illustrate what kind of an electron beam actually enters the ferromagnet. In the energy distribution curve $I(E)$ one distinguishes still an elastic peak at 7 eV, but secondary electrons have of course also been produced in Au at lower energies. However, the spin polarization of the elastic electrons is not altered on passing through the Au film. Yet the secondaries having suffered collisions with valence electrons in Au have a lowered polarization that decreases with decreasing energy due to the increasing admixture of unpolarized electrons excited from the conduction bands of Au.

The inset at the right shows data when a Co film of thickness $y = 4$ nm with its Au capping is added. One observes two different energy distribution curves of the emerging electron beam. I^+ is valid for $\vec{P}_0$ parallel and I^- for $\vec{P}_0$ antiparallel to $\vec{M}$, where the direction of $\vec{M}$ is defined by the direction of the majority spins. The elastic part of the beam displays a huge spin asymmetry $A = (I^+ - I^-)/(I^+ + I^-)$ for a pure spin state. On the other hand, the inelastic part of the electron spectrum exhibits lower A. This is partly due to the lower polarization of the inelastic electrons generated in the supporting Au layer. In the following, we focus on the elastic part of the spectrum which we can separate by applying a retarding field.

The most important condition for observing the large A is that the trilayer must have absolutely no holes. This is evident from Fig. 2, where the relative intensity transmitted through the Au/Co/Au is shown vs the energy E of the incident electron beam. The attenuation increases by 3 orders of magnitude when E increases from 6 eV above E_F to 16 eV. If there is the tiniest hole, the main part of the elastic signal observed at the back side of the trilayer is caused by electrons that have passed through the hole. We suspect that this is the reason why much smaller A values were reported in Ref. [14] at higher electron energies. The steep increase of the attenuation with increasing E is in reasonable agreement with the energy dependence of the electron mean free path in Au [15].

We now consider the attenuation of the elastic electron beam in the Co film of thickness y for each spin direction separately. With the incident current I_0 the transmitted current is $I = I_0 e^{-\sigma y}$. The absorption coefficient σ depends on the angle ϕ between $\vec{P}_0$ and $\vec{M}$; the largest value σ^- occurs with $\phi = \pi$ and the smallest

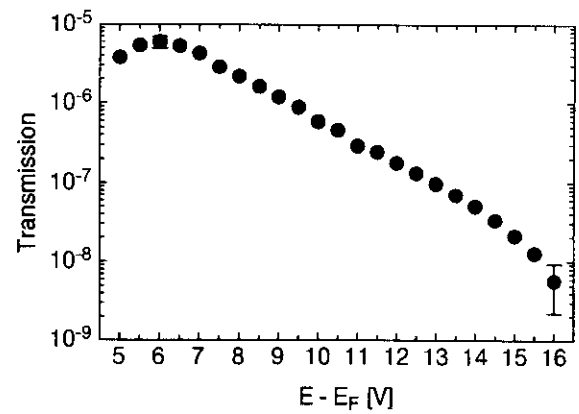

FIG. 2. The attenuation of the elastic electrons after penetration of the trilayer vs the energy above the Fermi energy E_F.

σ^+ with $\phi = 0$. With $\Delta\sigma = \sigma^- - \sigma^+$, we have $A = [\exp(\Delta\sigma y) - 1]/[\exp(\Delta\sigma y) + 1]$. One obtains

$$\Delta\sigma = \frac{1}{y} \ln\left(\frac{I^+}{I^-}\right). \quad (1)$$

Figure 3 shows a number of data obtained with various samples. To interpret this further, we assume that all of the spin-dependent scattering is scattering on the d shell, and that the strength of the scattering is proportional to the number of holes in that shell. The number of holes in the d shell is not *a priori* known for atoms in a metal. However, with the ferromagnetic metals, one knows the spin part of the saturation magnetization which is the difference in the occupancy of the d shell between majority- and minority-spin electrons known as the number of Bohr magnetons, n_B, per atom. With the present electron energies several eV above E_F, all of the d holes are available for scattering. This yields $\Delta\sigma = n_B\sigma_d$, where σ_d is the absorption coefficient for one unoccupied state in the $3d$ shell in Co. This approach is well supported by a number of quite different experiments [16].

With hcp Co, the density of atoms is $N = 8.6 \times 10^{28}$ atoms/m^3 and $n_B = 1.7$ Bohr magnetons. Hence, one obtains the following for the total scattering cross section:

$$Q = \frac{1}{Nn_B y} \ln\left(\frac{I^+}{I^-}\right). \quad (2)$$

The lower part of Fig. 3 shows Q calculated from the average of $\Delta\sigma$. The order of magnitude of Q reflects the fact that the d shell is comparatively little extended in space. For the interpretation one must be aware that Q is the sum of all scattering on the d shell, elastic and inelastic. Gokhale and Mills [17] have shown on the example of a single crystalline Fe film that effects of elastic scattering plus crystal diffraction and channeling can lead to sizable contributions to the spin-dependent transmission. However, these contributions favor both majority-spin and minority-spin transmission depending on the energy. Furthermore, they are generally not as large as observed here and also tend to increase on increasing the electron energy above 10 eV. Furthermore, crystal diffraction must cancel out for truly polycrystalline samples. We believe therefore that the main contribution to the total scattering cross section Q in Fig. 3 obtained from the average of $\Delta\sigma$ on all polycrystalline samples reflects predominantly the inelastic scattering on the d shell.

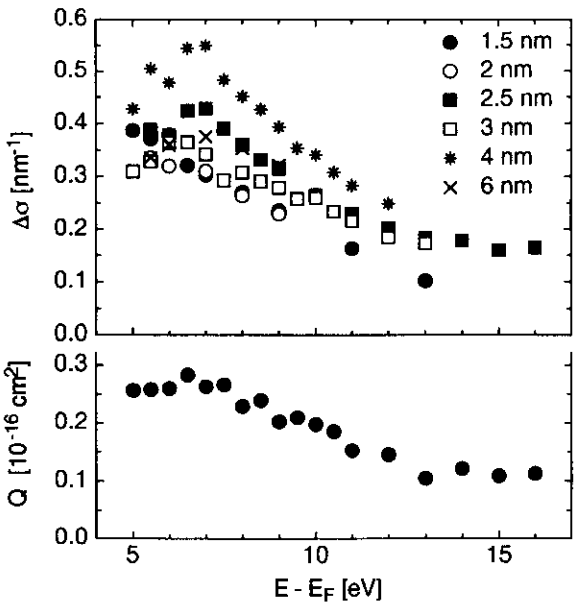

FIG. 3. Difference in the absorption coefficient $\Delta\sigma$ for majority- and minority-spin electrons vs electron energy for six samples each with a different Co thickness. The lower graph shows the average total scattering cross section Q for one hole in the $3d$ shell of Co.

To analyze the spin-selective scattering in ferromagnets in more depth, one must ask the question of what happens after the minority-spin electron has scattered into a hole of the d shell forming one of the $3d^{n+1}$ multiplet states. It has been argued [18] that the excess energy is dissipated by reemitting a majority-spin electron which, however, has lost at least the energy of the Stoner gap δ. In total, this process, called a Stoner excitation, would have made out of a minority spin in the primary electron beam a majority spin with a small energy loss δ. Such Stoner excitations have been detected experimentally [19,20]. We can test how important these excitations are in the spin-polarized transmission by making use of the theorem that a polarizing spin filter must be equal to an analyzing spin filter in the absence of spin-productive scattering events such as Stoner excitations [21]. The change in the majority-spin current is $dI^+ = -\sigma^+ I^+ dy - \alpha dI^-$, and in the minority-spin current $dI^- = -\sigma^- I^- dy$, where α is a constant. The fraction of minority-spin electrons that has undergone a spin flip in a Stoner excitation but is still detected in the elastic channel because δ is small, typically a fraction of an eV, is given by $r = \alpha/(1 - \alpha + \sigma^+/\sigma^-)$. The polarization P of an unpolarized electron beam passing through the ferromagnet will be

$$P = A + P^*(A, r, y), \quad (3)$$

while it is $P = A$ for $r = 0$. Experimentally, the comparison of P and A shows that the contribution of Stoner excitations r is below 5% and thus of minor importance in spin-dependent transmission.

We now consider the situation in which $\vec{P}_0$ is perpendicular to $\vec{M}$. In this case the spin part of the incident electron wave function can be described as a coherent superposition of a majority-spin ($\vec{s}$ parallel to $\vec{M}$) and a minority-spin ($\vec{s}$ antiparallel to $\vec{M}$) wave function with equal amplitudes: $\psi_0 = \frac{1}{\sqrt{2}}[\binom{1}{0} + \binom{0}{1}]$. Because of spin-dependent absorption, the amplitude of the two wave functions becomes different on passing the ferromagnet.

A phase difference ϵ develops as well. This yields the following for the wave function ψ of the electrons leaving the ferromagnet:

$$\psi = \frac{1}{\sqrt{2}}\left[\sqrt{1+A}\begin{pmatrix}1\\0\end{pmatrix}e^{-i\epsilon/2} + \sqrt{1-A}\begin{pmatrix}0\\1\end{pmatrix}e^{+i\epsilon/2}\right].$$

The spin polarization vector $\vec{P}$ of the transmitted electrons is determined by the expectation values of the Pauli matrices. (Note that the x axis is parallel to $\vec{P}_0$, the y axis is parallel to the electron beam, and the z axis is parallel to $\vec{M}$.) This yields

$$\vec{P} = \begin{pmatrix} P_0\sqrt{1-A^2}\cos(\epsilon) \\ P_0\sqrt{1-A^2}\sin(\epsilon) \\ A \end{pmatrix}, \tag{4}$$

and corresponds to two types of motion of the spin polarization vector, namely, a rotation by an angle of ϕ into the direction of $\vec{M}$ and a precession by an angle of ϵ around $\vec{M}$.

The rotation takes place in the plane spanned by $\vec{P}$ and $\vec{M}$. This rotation is due to absorption in the ferromagnetic film, as discussed above, where the minority-spin wave function is more strongly attenuated than the majority-spin wave function. The angle ϕ of the rotation is given by

$$\tan\phi = \frac{A}{P_0\sqrt{1-A^2}}. \tag{5}$$

The direct measurement of ϕ confirms Eq. (5). For example, for a Co film with $A = 0.3$, ϕ for a pure spin state is $\approx 17°$.

The precession around $\vec{M}$ is the electron analog to the Faraday rotation observed with linearly polarized light. It is a quantity that does not depend on A but is caused by the phase difference that develops between majority- and minority-spin wave functions due to the spin dependence of the inner potential. We found that the precession angle ϵ is $16 \pm 2°$ per 1 nm of Co film thickness for an electron energy of 7 eV. It will be discussed in more detail elsewhere.

In conclusion, we note that the very strong spin dependence of the transmission observed in polycrystalline hcp Co opens up the possibility to construct highly efficient spin filters, and to determine the Bohr magneton number n_B of thin films. Furthermore, the precession ϵ around the direction of $\vec{M}$ is unique because it measures the spin dependence of the inner potential otherwise inaccessible. The overall motion of the electron spin observed here is important for the understanding of ultrafast magnetization dynamics. The angles ϕ and ϵ are large considering that, depending on energy, the electrons spend only $\sim 0.3 \times 10^{-15}$ sec per nanometer film thickness within the ferromagnet.

We thank K. Brunner for expert technical assistance and D. Scheiwiller and Professor H. Baltes for helping us with the Si wafers. We are grateful to the Swiss National Science Foundation for having generously supported this project.

[1] U. Bänninger *et al.*, Phys. Rev. Lett. **25**, 585 (1970).
[2] P. W. Anderson, Philos. Mag. **24**, 203 (1971).
[3] S. Doniach, in *Magnetism and Magnetic Materials*, edited by D. C. Graham and J. J. Rhyne, AIP Conf. Proc. No. 5 (AIP, New York, 1971), p. 549.
[4] M. C. Gutzwiler, in *Magnetism and Magnetic Materials*, edited by C. D. Graham and J. J. Rhyne, AIP Conf. Proc. No. 10 (AIP, New York, 1972), p. 1197.
[5] For a review, see L. Kleinman, Comments Solid State Phys. **10**, 29 (1981).
[6] G. Busch *et al.*, Phys. Rev. Lett. **28**, 611 (1972).
[7] J. C. Gröbli *et al.*, Physica (Amsterdam) **204B**, 359 (1995).
[8] H. C. Siegmann, J. Electron Spectrosc. Relat. Phenom. **68**, 505 (1994).
[9] A. Filipe *et al.*, Phys. Rev. Lett. **80**, 2425 (1998), and references therein.
[10] J. Hohlfeld *et al.*, Phys. Rev. Lett. **78**, 4861 (1997).
[11] M. Aeschlimann *et al.*, Phys. Rev. Lett. **79**, 5158 (1997).
[12] A. Scholl *et al.*, Phys. Rev. Lett. **79**, 5146 (1997).
[13] Ganping Ju *et al.*, Phys. Rev. B **57**, R700 (1998).
[14] H. J. Drouhin *et al.*, J. Appl. Phys. **79**, 4734 (1996).
[15] O. Paul, Dissertation ETH Zurich No. 9210, 1990.
[16] H. C. Siegmann, *Selected Topics on Electron Physics*, edited by M. Campbell and H. Kleinpoppen (Plenum, New York, 1996).
[17] M. P. Gokhale and D. L. Mills, Phys. Rev. Lett. **66**, 2251 (1991), and references therein.
[18] J. Glazer and E. Tosatti, Solid State Commun. **52**, 905 (1984).
[19] J. Kirschner, D. Rebenstorff, and H. Ibach, Phys. Rev. Lett. **53**, 698 (1984).
[20] H. Hopster, R. Raue, and R. Clauberg, Phys. Rev. Lett. **53**, 695 (1984).
[21] J. Kirschner, *Polarized Electrons at Surfaces*, Springer Tracts in Modern Physics Vol. 106 (Springer-Verlag, Berlin, 1985), p. 60.

spin, time, and energy analysis, will be presented elsewhere [20]. In brief, two equally intense, collinear, orthogonally polarized light pulses with an adjustable delay interact with the metal surface. The mutual orthogonal linear polarization of the two pulses suppresses coherent excitation to a large extent [18]. While the first pulse excites electrons from their ground state into an intermediate state below the vacuum level, the second pulse—after a delay—interacts with the still excited electrons. In this second step the electrons are excited above the vacuum level, so that they can be detected as photoelectrons. By measuring the photocurrent as a function of the delay between the two light pulses, the lifetime of the excited electrons at a fixed intermediate state energy is determined. We emphasize that this two pulse correlation experiment allows one to determine lifetimes which are considerably shorter than the duration of the laser pulse [18]. A Ti:sapphire laser operating at a repetition rate of 82 MHz and a pulse width of about 40 fs is used as a pulsed light source. The linearly polarized laser output is frequency doubled in a 0.2 mm thick beta barium borate crystal to produce UV pulses between 3 and 3.4 eV photon energy. We used laser pulses of low fluence and peak power in order to avoid space charge effects on the energy distribution of the electrons. In this way, the relaxation of individual excited electrons rather than the collective behavior of a transiently heated nonequilibrium distribution is measured. Note that the count rate is much lower than one electron per pulse.

The two photon-photoemission (2PPE) experiments are performed in an ultrahigh vacuum system equipped with a cylindrical sector energy analyzer. The orientation of the sample is 45° with respect to the laser beam, and the electrons are detected in normal emission geometry. Epitaxial fcc Co films, about 10 nm thick, are grown onto a Cu(001) single crystal at room temperature [21]. The growth rate is 0.2 nm/min. The thickness of the film is measured by a calibrated quartz microbalance. Remanent magnetization of the Co(001) films is achieved by magnetizing them by a magnetic field pulse from a coil. The easy axes of the magnetization in Co/Cu(001) are shown to be the in-plane [110] directions [22]. The geometry of the system allows the measurement of the projection of the spin polarization vector along the in-plane Co [110] direction: $P = (N^{\uparrow} - N^{\downarrow})/(N^{\uparrow} + N^{\downarrow})$ with $N^{\uparrow}$ ($N^{\downarrow}$) the number of photoemitted electrons with their magnetic moment parallel (antiparallel) to the sample magnetization. The lowest available intermediate state energy that can be probed is given by $\Phi - h\nu$, with Φ being the work function of clean Co(001) ($\approx$5 eV) and $h\nu$ the photon energy. In order to extend the energy range to lower energies, we can reduce the work function by depositing small amounts ($\leq$0.1 ML) of Cs onto the Co surface. The effect of Cs on the electron scattering is negligible: within the present time resolution we do not observe a difference in the spin-integrated lifetime measurements between a clean Co surface and a Cs/Co surface in the overlapping energy region between 1.7 and 3.3 eV.

A normal emission 2PPE spectrum of a cesiated 10 nm thick Co(001) film with one laser beam blocked (i.e., without time resolution) at a photon energy of 3 eV is shown in Fig. 1. The electron energy values correspond to the actual kinetic energy of the free photoelectron: $E_{kin} = 2h\nu - \Phi - E_i$ with E_i being the initial state energy below E_F; the shift due to the difference in the work function between the sample and the detector has been compensated and the applied bias subtracted. The peak at the largest kinetic energies is built up by electrons coming from the vicinity of E_F, where Co 3*d* emission is strongest. That this structure is actually built up by Co 3*d* emission can be seen easily by the strong increase in the 2PPE intensity upon the subsequent evaporation of Co on the Cu substrate. The enhancement of the 2PPE yield at lower energies, on the other hand, is not due to an intrinsic feature of the Co band structure. Instead, this increase is due to the increase in the lifetime of the intermediate states at lower energies (see Fig. 2) and also to the buildup of the secondary electron cascade. The population of a state may be refilled through inelastic collisions of excited electrons in energetically higher lying states. The open squares in Fig. 1 represent the spin polarization of the photoemitted electrons. In spite of the quite structured spin-dependent density of states of Co (see inset in Fig. 3), the spin polarization does not show very much structure. Even more remarkable, the maximum spin polarization value is about 65%, which is 1.5 times higher than values obtained in single photon threshold photoemission experiments [23]. The occurrence of this

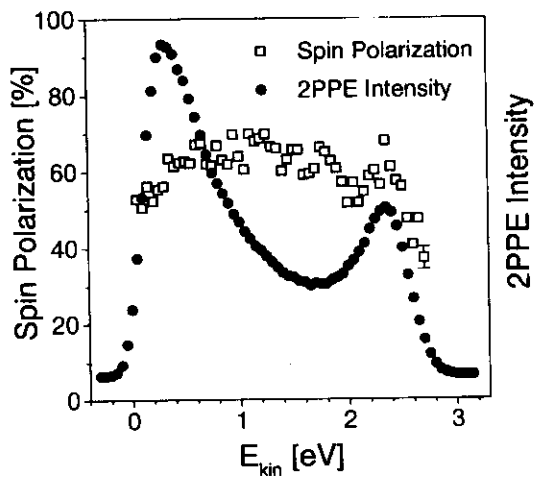

FIG. 1. Intensity (filled circles) and spin polarization (open squares) of a cesiated 10 nm thick Co(001) film as a function of the kinetic energy, obtained in a 2PPE experiment with one laser beam blocked. The photon energy of the laser light is 3 eV. The work function of this particular cesiated sample is 3.4 eV.

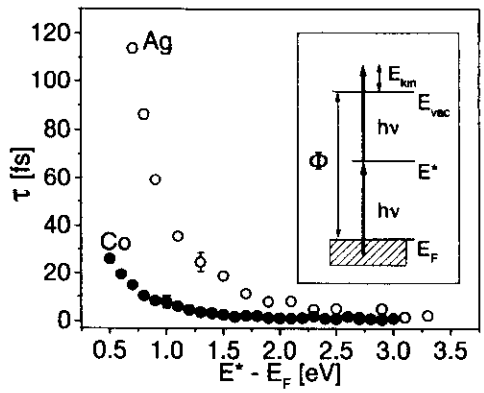

FIG. 2. The spin-integrated inelastic lifetime of cesiated Co(001) ($h\nu = 3$ eV, $\Phi = 3.5$ eV) and Ag(111) ($h\nu = 3.3$ eV, $\Phi = 4.1$ eV) as a function of the intermediate state energy above E_F. The inset shows a scheme of the energy levels involved in the 2PPE process.

enhanced spin polarization is consistent with the existence of a spin filter effect in Co, as it preferentially depletes the population of the excited minority-spin electrons during the first and the second excitation process. However, the large spin polarization of the 2PPE yield is not a conclusive proof of the spin filter effect, since different excitation processes and, hence, transition matrix elements have to be considered in 2PPE compared to regular photoemission induced by absorption of a single photon.

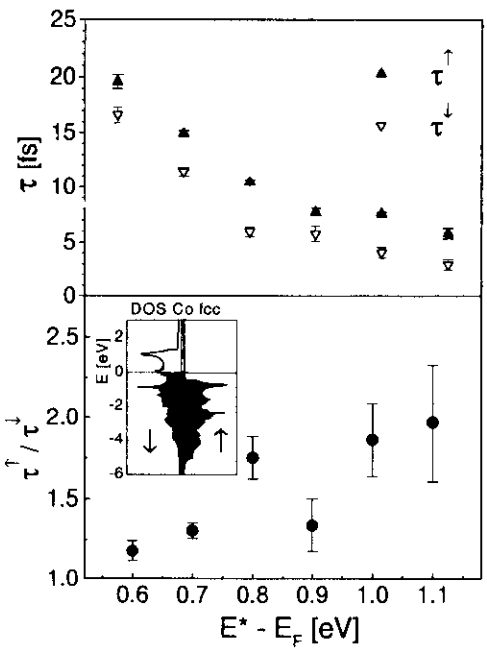

FIG. 3. The spin-resolved inelastic lifetime (top) and the ratio $\tau^{\uparrow}/\tau^{\downarrow}$ (bottom) of a cesiated 10 nm thick Co(001) film as a function of the intermediate state energy above E_F. In the top panel filled symbols correspond to the majority-spin direction and open symbols to the minority-spin direction. The photon energy is 3 eV. The inset in the bottom panel shows the spin-resolved density of states of fcc Co [26].

The marked drop in P at the highest kinetic energies (corresponding to initial state energies around E_F) is consistent with single photon threshold photoemission experiments on thick Co(001) films, where P decreases from 40% to 20% on approaching the photothreshold [23]. This decrease in P has been attributed to the fact that Co is a strong ferromagnet and, hence, has no majority-spin d density of states at E_F. That P is positive even at the photothreshold has been one of the main arguments for the spin filter process [23]. At the lowest kinetic energies in the 2PPE spectrum, however, the drop in P might be generated by the growing importance of secondary electrons.

Figure 2 shows the spin-integrated lifetime τ of both cesiated Co and the noble metal Ag for comparison as a function of the intermediate state energy E^*. The data are extracted from the experimentally obtained cross-correlation traces using a rate equation model for the population of the intermediate state [20]. This model is equivalent to the Bloch equations for a three level system in the limit of rapid dephasing [24]. In this case, the evolution of the transient population $N^*(t)$ of the intermediate level is given by $dN^*(t)/dt = A(t) - N^*(t)/\tau$, where $A(t)$ is the excitation induced by the first (pump) laser pulse. It should be noted, however, that the depletion of a photoexcited population at E^* is governed not only by an energy-dependent lifetime. At lower energies, the cross-correlation signal is affected both by secondary electrons (cascade and Auger electrons) and transport processes. Secondary electrons repopulate the probed state, whereas the diffusion of the electrons out of the probed region (transport) depopulate the state. These two opposed contributions are not involved in the rate equation model and therefore neglected in this first interpretation. The lifetime curves for both Co and Ag show a clear increase in lifetime on approaching E_F. The cause for this increase in lifetime is the decreasing phase space that is available for scattering processes. Within the framework of a conventional Fermi liquid theory, a $1/(E^* - E_F)^2$ behavior is expected [25], which is in fair agreement with the observations displayed in Fig. 2. On the other hand, the lifetimes in Co are much shorter than in Ag. In the noble metal Ag, the d band is completely filled, while the d band of the transition metal Co is only partially filled, and relaxation is dominated by the d electrons. The higher density of occupied and unoccupied states near E_F in Co is thus seen to lead to a faster relaxation and hence to shorter inelastic lifetimes.

In the top panel of Fig. 3, the spin-dependent lifetime of Co as a function of the intermediate state energy between 0.6 and 1.1 eV above E_F is shown. Each pair of data points is the result of $\approx$10 h of measuring time. Clear lifetime differences between the two spin states are found, resulting in a longer lifetime of majority-spin electrons. The error bars in the plot represent the statistical scatter as described in Ref. [20]. Besides the pure statistical

error, one important additional source of error is the determination of the zero point of the lifetime scale. Thus the absolute values of the lifetimes are correct only within a few femtoseconds [18]. However, this does not influence the lifetime difference found for the two spin channels, because both were measured simultaneously. The qualitative behavior of the spin-dependent lifetime, namely, the longer lifetime of majority-spin electrons, can readily be explained by the excess of unfilled minority-spin states compared to unfilled majority-spin states, as discussed above. Because of the larger number of minority-spin holes, the minority-spin electrons are scattered out of a given energy at a faster rate than majority-spin electrons. Explaining the details of the curve is obviously more complicated and requires as the next step that the actual electronic band structure of Co(001) be taken into consideration. In the bottom panel of Fig. 3 the lifetime ratio $\tau^{\uparrow}/\tau^{\downarrow}$ is plotted, exhibiting a value of roughly 2 at 1 eV above E_F. A decreasing ratio is found towards lower energies. We note that the spin-resolved measurements are stopped at 1.1 eV, because the errors bars are getting too large due to the short lifetimes, which are at the limit of our present time resolution. A look at the Co density of states [26] (see inset) might give a clue about the behavior of the lifetime ratio. For intermediate state energies above $\approx$1.3 eV, all empty d states, in particular those which build up the strong density of states peak at around 1 eV, are available for minority-spin electrons to scatter into. For intermediate state energies clearly below 1 eV, however, the strong density of states peak is no longer available for the scattering of minority-spin electrons. Since the phase space for scattering of majority-spin electrons, on the other hand, does not change as much as in the case of minority-spin electrons—due to the constant majority-spin density of states in the energy range of interest—the lifetime ratio should change in favor of the minority-spin electron lifetime at lower energies.

In conclusion, by combining time- and spin-resolved photoemission techniques, we have demonstrated that the spin-dependent dynamics of optically excited electrons can be studied in real time. The spin-dependent lifetime of electrons in Co(001) is determined directly from the experiment and is found to be larger for majority-spin electrons than for minority-spin electrons. It is hoped that these experiments will contribute to a better understanding of spin-dependent scattering, which is of eminent importance for understanding transport properties in magnetic materials as well as the process of photoemission at low photon energies. There are also a number of applications of the spin filter effect in ferromagnets such as, for instance, the possibility to build very efficient detectors for electron spin polarization opening up the possibility to apply spin-polarized electrons more widely. At any rate, this experiment provides the first information on the spin-dependent lifetimes in the energy range between the Fermi energy and the vacuum level, thereby closing the gap between information from electric transport and mean free path experiments.

We thank P. Apell, M. Donath, P. Echenique, and M. Landolt for many helpful discussions. We thank R. Allenspach for lending us the Cu single crystal. This work was supported by the Swiss National Science Foundation (Grant No. 21-39385.93).

[1] M. N. Baibich *et al.*, Phys. Rev. Lett. **61**, 2472 (1988).
[2] J. Unguris *et al.*, Phys. Rev. Lett. **49**, 72 (1982).
[3] E. Kisker, W. Gudat, and K. Schröder, Solid State Commun. **44**, 591 (1982).
[4] H. Hopster *et al.*, Phys. Rev. Lett. **50**, 70 (1983).
[5] D. P. Pappas *et al.*, Phys. Rev. Lett. **66**, 504 (1991).
[6] M. Getzlaff, J. Bansmann, and G. Schönhense, Solid State Commun. **87**, 467 (1993).
[7] R. J. Celotta, J. Unguris, and D. T. Pierce, J. Appl. Phys. **75**, 6452 (1994).
[8] F. Sirotti, G. Panaccione, and G. Rossi, J. Phys. (Paris), Colloq. **4**, C9-175 (1994).
[9] J. C. Gröbli, D. Oberli, and F. Meier, Phys. Rev. B **52**, R13095 (1995).
[10] E. Vescovo *et al.*, Phys. Rev. B **52**, 13 497 (1995).
[11] F. Passek, M. Donath, and K. Ertl, J. Magn. Magn. Mater. **159**, 103 (1996).
[12] H. C. Siegmann, in *Selected Topics in Electron Physics*, edited by M. Campbell and H. Kleinpoppen (Plenum Press, New York, 1996).
[13] J. Glazer and E. Tosatti, Solid State Commun. **52**, 905 (1984).
[14] D. R. Penn, S. P. Apell, and S. M. Girvin, Phys. Rev. B **32**, 7753 (1985).
[15] M. P. Gokhale and D. L. Mills, Phys. Rev. Lett. **66**, 2251 (1991).
[16] G. Schönhense and H. C. Siegmann, Ann. Phys. (Leipzig) **2**, 465 (1993).
[17] F. Passek *et al.*, Phys. Rev. Lett. **75**, 2746 (1995).
[18] M. Aeschlimann, M. Bauer, and S. Pawlik, Chem. Phys. **205**, 127 (1996).
[19] The spin analyzer used in this study is a so-called "LEED"-detector, the functioning of which is based on the spin-orbit scattering of low energetic electrons in W(001) [see J. Kirschner, in *Polarized Electrons in Surface Physics*, edited by R. Feder (World Scientific, Singapore, 1985), Chap. 5.2].
[20] M. Aeschlimann *et al.* (to be published).
[21] W. Weber *et al.*, Phys. Rev. B **54**, 4075 (1996).
[22] D. Kerkmann *et al.*, Solid State Commun. **72**, 963 (1989).
[23] J. C. Gröbli *et al.*, Physica (Amsterdam) **204B**, 359 (1995).
[24] E. Knoesel *et al.*, Surf. Sci. **368**, 76 (1996).
[25] J. J. Quinn, Phys. Rev. **126**, 1453 (1962).
[26] We thank W. Wolf and J. Noffke for providing band structure calculations of fcc Co.